

THE COMPUTATION OF BUOYANT FLOWS IN DIFFERENTIALLY HEATED VERTICAL AND INCLINED CAVITIES

Tim J Craft, Hector Iacovides, Ali Omranian

Turbulence Mechanics Group,
School of Mechanical, Aerospace and Civil Engineering,
The University of Manchester, Manchester M60 1QD, UK
h.iacovides@manchester.ac.uk

ABSTRACT

This study explores the potential of a recently developed wall-function strategy, based on the analytical solution of simplified, boundary-layer, forms of the momentum and enthalpy transport equations, for the economical and reliable prediction of natural convection flows. Comparisons are also drawn with results from the conventional wall-function strategy, based on the log-law. These near-wall modelling strategies have been combined with different high-Reynolds-number turbulence models, including the $k-\varepsilon$, a basic form of 2nd-moment closure, and a more elaborate version, which satisfies certain physical realizability constraints. In the 2nd-moment computations, in addition to the generalized gradient diffusion hypothesis, more complex algebraic forms have also been employed for modelling the turbulent heat fluxes, involving the solution of transport equations for the temperature variance and its dissipation rate. Four test cases have been computed: a square cavity with differentially heated vertical walls, and a tall cavity with similar heating arrangements at three different angles of inclination; vertical, 60° and 5° to the horizontal. The resulting comparisons show that the more elaborate wall function shows distinct predictive advantages, and in some cases even returns superior predictions to a low-Re model. The $k-\varepsilon$ model, when used with the new near-wall approach, is satisfactory in most cases. Of the second-moment closures, the realizable version, used with the more complex thermal field models, yields the most satisfactory flow and thermal predictions.

INTRODUCTION

Natural convection flows are encountered in nature and also in engineering applications, including domestic heating, refrigeration and nuclear reactor cooling systems. The fluid motion and thereby the thermal convection process, are driven by the gravitational force acting in regions of variable fluid temperature and consequently density. The fact that in cases of natural convection the Nusselt number can be considerably higher than unity shows that buoyancy-induced motion can significantly enhance the wall heat transfer. The process can be characterised by either the Grashoff, or the Rayleigh number $Ra \equiv gPr\beta(\Theta_H - \Theta_C)L^3/\nu^2$. As the Rayleigh number increases, the buoyancy-driven flow undergoes transition from laminar to turbulent, leading to even greater enhancement in wall heat transfer.

Turbulent natural convection flows, in even simple systems, can be physically complex. The buoyancy force influences the turbulence field directly and, depending on the orientation of the temperature gradients, can either

generate or suppress turbulence. The computation of turbulent buoyant flows is a challenge. It has long been recognised that, due to the gravitational body force, natural convection boundary layers do not follow the “universal” log-law. Most attempts to compute turbulent natural convection flows have thus avoided use of the traditional wall-function approach for the prescription of wall boundary conditions, because this involves the assumption of logarithmic wall laws. Ince and Launder (1989) examined natural convection flows in tall differentially heated cavities using a low-Re $k-\varepsilon$ scheme with the generalised gradient diffusion hypothesis (GGDH) modelling of the turbulent heat fluxes. Professor Hanjalic’s group has made a series of contributions to this topic. In Hanjalic (1994), Hanjalic et al (1996), Dol et al (1997) and Kenjeres and Hanjalic (1999) a range of natural convection flows were studied, including empty and partitioned rectangular enclosures and Rayleigh-Benard cells. They found it necessary to extend the low-Reynolds-number $k-\varepsilon$ model to include more complex algebraic equations for the turbulent stresses and heat fluxes, requiring transport equations for the temperature variance $\overline{\theta^2}$ and its dissipation rate ε_θ .

The authors’ group has developed more general wall-functions. While retaining the numerical robustness of the conventional, “standard” approach, these no longer need to assume logarithmic variations of the near-wall velocity and temperature. One such strategy, the analytical wall function (AWF) of Craft et al (2002), has been employed successfully in mixed convection flows. For the outer field Craft and Launder (2001) developed a refined 2nd-moment closure, using realizability constraints which satisfy the 2-component limit of turbulence (TCL). As subsequently shown by Craft et al (2004), in the computation of buoyancy-opposed wall jets this TCL 2nd-moment closure led to predictive improvements in comparison to the “Basic” one of Gibson and Launder (1978).

Here the main aim is to assess the effectiveness of the analytical wall function (AWF), Craft et al (2002), for the modelling of the near-wall turbulence in the computation of natural convection flows. This is done in conjunction with a high-Re $k-\varepsilon$ scheme and two 2nd-moment closures (the original, “Basic”, closure and more recent TCL version) for the outer field. With these latter schemes algebraic equations for the turbulent heat fluxes, which involve

transport equations for the temperature variance $\overline{\theta^2}$ and its dissipation rate ε_θ , are also adopted. Comparisons are drawn with experimental data and results using a standard wall-function (SWF) approach.

Four cases have been investigated: one square and three tall rectangular differentially heated cavities. The square cavity was experimentally investigated by Ampofo and Karayiannis (2003). The tall cavity cases involve three orientations: a vertical cavity, (measurements from Betts and Bokhari, 2000); one inclined at an angle of 60° to the horizontal (experimental data by Esteifi, 2008), and one inclined at 5° to the horizontal (LES data by Addad et al, 2008). The latter two both have a heated upper surface.

TURBULENCE MODELLING

Modelling of Turbulent Stresses and Heat Fluxes

Most computations employed high-Reynolds-number models, in which the dynamic and thermal turbulence fields are determined from the solution of transport equations and wall boundary conditions are specified from a knowledge of near-wall turbulence, to avoid the need for fine near-wall grids. The models tested are listed in Table 1.

k-ε Models

The effective viscosity and diffusivity approximations are

$$\overline{u_i u_j} = \frac{2}{3} k \delta_{ij} - \nu_t \left(\frac{\partial U_i}{\partial x_j} + \frac{\partial U_j}{\partial x_i} \right) \quad \overline{u_i \theta} = - \frac{\nu_t}{\sigma_\theta} \frac{\partial \Theta}{\partial x_i} \quad (1)$$

with the turbulent viscosity taken as $\nu_t = c_\mu f_\mu k^2 / \epsilon$, and the turbulent kinetic energy, k , and its dissipation rate, ϵ , obtained from separate transport equations.

Second-Moment Closure (RSM) Models

The Reynolds stresses are now obtained using transport equations of the type shown below:

$$\frac{\partial}{\partial x_k} (\rho U_k \overline{u_i u_j}) = d_{ij} + P_{ij} + G_{ij} + \Phi_{ij} - \rho \epsilon_{ij} \quad (2)$$

$$P_{ij} = -\rho \left(\overline{u_i u_k} \frac{\partial U_j}{\partial x_k} + \overline{u_j u_k} \frac{\partial U_i}{\partial x_k} \right) \quad (3)$$

$$G_{ij} = -\rho \beta \left(g_i \overline{u_j \theta} + g_j \overline{u_i \theta} \right) \quad (4)$$

The generation rate terms, P_{ij} , due to shear, and G_{ij} , due to the buoyancy force, are exact. Terms d_{ij} , Φ_{ij} and ϵ_{ij} require modelling. Different approximations to these terms are adopted in the two RSM models, Basic and TCL. The two RSM models also adopt different forms for the transport equation for the dissipation rate, ϵ . It is worth noting the buoyant generation rate term, G_{ij} , for two reasons. First, according to how the turbulent heat flux vector is aligned with the vertical it can be either positive or negative, enhancing turbulence when the temperature increases in the downward direction, and attenuating turbulence when the temperature gradient is reversed. Second, even though its trace ($G_{11}+G_{22}+G_{33}$) is non-zero and hence also present in effective-viscosity models, it is highly anisotropic in its effect. This feature can only be reproduced by second-moment closures.

Generalised Gradient Diffusion Hypothesis

This representation of the turbulent heat fluxes is usually employed with second-moment closures:

$$\overline{u_i \theta} = -c_\theta \frac{k}{\epsilon} \overline{u_i u_k} \frac{\partial \Theta}{\partial x_k} \quad (5)$$

Table 1. Summary of turbulence models tested.

Reynolds Stresses	Turbulent Heat Fluxes	Near-Wall Strategy	Name
Low-Re $k-\epsilon$, Launder-Sharma	Effective Diffusivity	Low-Re Model. Fine grid	LRN
High-Re $k-\epsilon$	Effective Diffusivity	Standard Wall Funct.	SWF
High-Re $k-\epsilon$	Effective Diffusivity	Analytical Wall Funct.	AWF
Diff. Model. Gibson-Launder	Generalised Gradient Diffusion Hypothesis	Analytical Wall Function	RSM Basic
Diff. Model. Gibson-Launder	Algebraic model eqns. for θ^2 and ϵ_θ . Hanjalic et al	Analytical Wall Function	Mod RSM Basic
Diff. Stress Model. Craft-Launder	Generalised Gradient Diff. Hypothesis	Analytical Wall Function	RSM TCL
Diff. Model. Craft-Launder	Algebraic model eqns for θ^2 and ϵ_θ . Hanjalic et al	Analytical Wall Function	Mod RSM TCL

Hanjalic et al (1996) Heat Flux Model

Here a more elaborate algebraic expression is used for the turbulent heat fluxes:

$$\overline{u_i \theta} = -c_\theta \frac{k}{\epsilon} \left(\overline{u_i u_j} \frac{\partial \Theta}{\partial x_j} + \xi \overline{u_j \theta} \frac{\partial U_i}{\partial x_j} + \eta \beta g_i \overline{\theta^2} \right) \quad (6)$$

The temperature variance, $\overline{\theta^2}$, which appears in these heat flux equations, is determined from additional transport equations for $\overline{\theta^2}$ and its dissipation rate ϵ_θ , not included here due to space limitations.

Modelling of Near-Wall Turbulence

The modelling of near-wall turbulence has been one of the focal points of this study. Effective-viscosity, $k-\epsilon$, computations have been performed with three different approaches: firstly a low-Reynolds-number model, secondly the conventional, “standard”, wall-function approach based on the log-law, and finally the more general analytical wall-function of Craft et al (2002). The low-Reynolds-number (LRN) model employed here is the Launder-Sharma (1974) model, which has been applied to the computation of natural convection flows with some success, Ince and Launder (1989), but which requires the use of fine near-wall grids.

The standard wall function “SWF”, is a well-documented approach, in which in order to avoid the need for fine near-wall grid resolution, a logarithmic velocity variation, the local equilibrium of turbulence and a constant turbulence shear stress are assumed across the near-wall control volumes. Wall boundary conditions to the mean momentum and enthalpy equations, and also to those for the transport of turbulence quantities such as k and ϵ , can then be specified from the values of the mean flow and turbulence parameters at the near-wall nodes. This approach is numerically robust, but lacks generality, due to the limitations imposed by the assumptions employed.

The analytical wall function, “AWF”, Craft et al (2002), removes some of the limiting assumptions of the standard approach, but without sacrificing its numerical robustness. As in the SWF, large near-wall control volumes are employed and wall boundary conditions to all transport equations are specified from the values of the mean flow

and turbulence parameters at the near-wall nodes. This process is, however, based on near-wall variations of the mean wall-parallel velocity and temperature which result from the analytical integration of simplified near-wall forms of their transport equations:

$$\frac{\partial}{\partial y} \left[\left(\frac{\mu}{Pr} + \frac{\mu_t}{\sigma_\theta} \right) \frac{\partial \Theta}{\partial y} \right] = \frac{\partial}{\partial x} (\rho U \Theta) + \frac{\partial}{\partial y} (\rho V \Theta) \quad (7)$$

$$\frac{\partial}{\partial y} \left[(\mu + \mu_t) \frac{\partial U}{\partial y} \right] = \frac{\partial (\rho U^2)}{\partial x} + \frac{\partial (\rho UV)}{\partial y} + \frac{\partial P}{\partial x} - \rho_{ref} g_x (\Theta - \Theta_{ref}) \quad (8)$$

The wall-parallel and wall-normal directions are denoted by x and y respectively. The turbulent viscosity, μ_t , is assumed to vary linearly across the near-wall cell according to:

$$\mu_t = \begin{cases} 0 & \text{for } y^* < y_v^* \\ c_\mu c_l \mu (y^* - y_v^*) & \text{for } y^* \geq y_v^* \end{cases} \quad (9)$$

where the dimensionless thickness of the zero-turbulent-viscosity sub-layer, y_v^* , is taken as 10.8.

The wall-parallel convection and pressure gradient terms in equations (7) and (8) are treated as constants and calculated from nodal values, while for the buoyancy term in equation (8) the variation produced by the solution of equation (7) is used. The wall-normal convection term, when the wall-normal velocity at the near wall cell is towards the wall, is treated as constant over the entire cell, while when the wall-normal velocity is away from the wall, a two-layer approach is adopted. In this case, outside the zero-turbulent-viscosity layer it is evaluated from the nodal values, whilst within the sub-layer velocity values at the edge of the sub-layer are used, based on linear interpolation.

The above strategy makes the introduction of further refinements possible, such as accounting for changes in molecular properties across the sub-layer. More details are given in Craft et al (2002).

CASES EXAMINED

Four cases of free convection flows in enclosed cavities have been computed, for which validation data are available. The first is that of flow in a square cavity with differentially heated vertical walls. Along the horizontal walls the temperature changes from that of the hot wall at one end to that of the cold at the other. The Rayleigh number value based on the side of the square cavity is 1.58×10^9 and the Prandtl number 0.7. The other three cases involve a tall cavity, aspect ratio 28.7, with one hot and one cold long wall and thermally insulated end walls at a Rayleigh number of 0.86×10^6 and a Prandtl number of 0.7. The first of the tall cavity cases is a vertical cavity with the long walls at 90° to the horizontal. The second is inclined at an angle of 60° to the horizontal, with the hot surface being the upper one and the third of the long cavity cases is at an angle of 5° to the horizontal, also with the upper surface being the hot surface.

NUMERICAL ASPECTS

The in-house, two-dimensional, code TEAM has been used. It is a finite volume, structured code which solves the heat and fluid flow equations in either Cartesian or axisymmetric co-ordinates with a staggered grid arrangement. In the case of the DSM computations, the apparent viscosity

concept was also employed to enhance numerical stability. For the discretization of convective transport the 3rd order upwind QUICK scheme was employed.

Following grid sensitivity tests, for the square cavity, the low-Re $k-\varepsilon$ results have been obtained using an 80×80 grid and for all computations employing high-Re models a 40×40 mesh has been employed, with y^* ($\equiv y k^{1/2} / \nu$) values at the near-wall nodes ranging from 3 to 40. For the tall cavity, low-Re $k-\varepsilon$ computations have been obtained with an 80×120 mesh and high-Re models employed a 20×80 mesh with y^* values ranging from 4 to 22.

RESULTS

Square Cavity

The differential heating generates the convection cell shown in Figure 1, in which there is a strong near-wall motion, with impingement regions at the four corners, but especially at the corner between the hot and upper walls and also the one diametrically opposite. The measurements of Ampofo and Karayiannis (2003) show that the flow is turbulent in the near-wall regions, but with a laminar core.

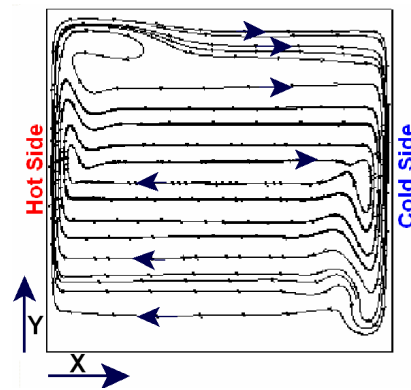


Figure 1. Streamlines in square cavity, $Ra = 1.58 \times 10^9$.

The comparisons of Figures 2 and 3, which focus on the boundary layer at the half-way point of the hot wall, are typical of a wider range of comparisons (at both vertical walls) and provide a good assessment of the different modelling strategies. Starting with the vertical velocity comparisons of Figure 2, the $k-\varepsilon$ predictions on the left hand side graph show that the low-Re model under-predicts the boundary layer thickness, suggesting that this model returns a laminar boundary layer, while the high-Re model with either wall function predicts the correct boundary layer thickness. Moreover, while the SWF version underestimates the velocity maximum, the AWF returns a value close to that measured. The Basic RSM, with the AWF, returns the correct velocity variation as well, while the TCL version appears to predict a thicker boundary layer and a lower velocity maximum. In the corresponding comparisons of the turbulent kinetic energy, k , of Figure 3, the $k-\varepsilon$ comparisons show that, as suggested by the velocity profiles, the low-Re model predicts zero k levels. The two high-Re versions, which return turbulent boundary layers, under-estimate the peak k level, but again the AWF predictions are closer to the measurements. Switching to the basic RSM, with the AWF, leads to further predictive improvements. Introducing the TCL version and the Hanjalic et al (1996) approximation of the heat fluxes,

causes the k levels to be over-estimated, though not severely. Introduction of transport equations for the temperature variance and its dissipation rate does not change the velocity predictions (not included here) but leads to a modest increase in the predicted k levels.

In Figure 4, $k-\epsilon$ predictions of the local Nusselt number over the walls of the square cavity are compared. The data show that the maximum levels occur at the bottom of the hot and the top of the cold walls, where Figure 1 shows flow impingement. These values are only captured with the AWF. The SWF produces a flatter Nu distribution. The low-Re model, which predicts laminar flow, under-estimates peak levels. The RSM, Figure 5, does not lead to significant improvements in local Nu predictions. The RSM-TCL, with the Hanjalic et al (1996) approximation of the heat fluxes, improves Nu predictions along the two horizontal walls.

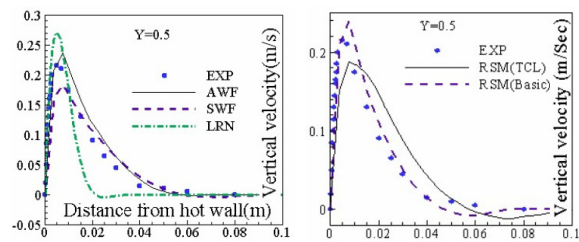


Figure 2. Vertical velocity variation along the mid-horizontal line near hot wall. Square cavity, $Ra=1.58 \times 10^9$.

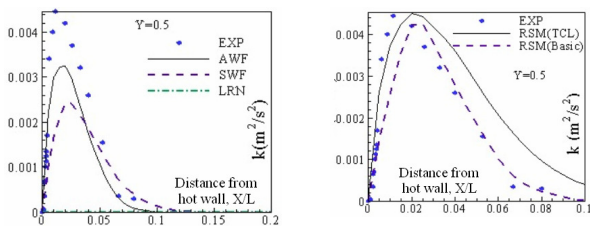


Figure 3. Turbulent kinetic energy along the mid-horizontal line near hot wall. Square cavity, $Ra=1.58 \times 10^9$.

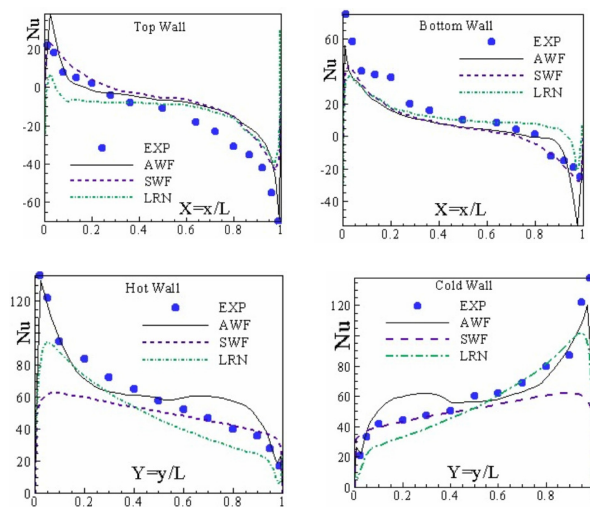


Figure 4. Local Nusselt number variation over the walls of the square cavity. $Ra = 1.58 \times 10^9$, $k-\epsilon$ comparisons.

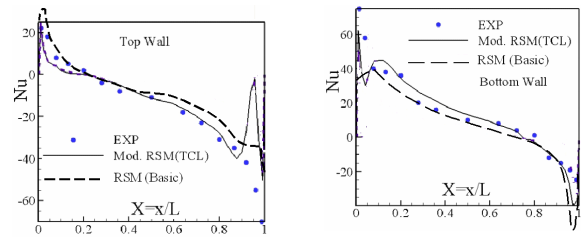


Figure 5. Local Nusselt number variation over the walls of the square cavity. $Ra = 1.58 \times 10^9$, RSM comparisons.

Tall Cavities

Figure 6 shows streamline plots of the three cases. The 90° and 60° cavities show very few differences in the mean flow which are confined to the end-wall regions. The 5° cavity displays a different behaviour, with the recirculation cell confined to the middle third of the cavity and having a different inclination angle to that of the cavity.

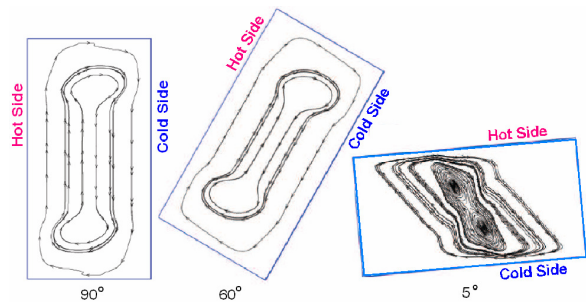


Figure 6. Mean flow fields in 90° and 60° tall cavities, $Ra=0.8 \times 10^6$.

Similarities in the flow development at the 90° and 60° angles are also evident in the temperature profile comparisons of Figure 7. At both angles the temperature variation over the middle cavity region is determined by turbulent mixing, while near the end walls it is mainly influenced by convection. In contrast to the square cavity, for all the versions of the $k-\epsilon$ model the mean temperature predictions agree with each other and also with the data. The RSM comparisons, Figure 8, show that the basic RSM also returns reliable temperature predictions throughout these two cavities, while the two-component-limit version appears to over-estimate turbulence mixing near the end walls. The more elaborate heat flux model improves the thermal predictions of the RSM-TCL, but differences with the data still remain. For the vertical cavity, Figure 9, the mean velocity across the middle region is well predicted. The only exception is the basic RSM, which over-predicts the velocity peaks. Local Nu comparisons for the 90° case, Figure 10, show that all EVM models return the correct Nu variation. Comparisons with RSM predictions, not included, show similar agreement with the data.

Figure 11 focuses on temperature variance at the cavity mid-height. For the 90° case, the extended RSM, which includes a transport equation for the temperature variance, predicts the correct levels in the cavity core, but higher near-wall levels. For the 60° case, the experiments show a reduction in the level of temperature fluctuations, possibly due to the stable stratification. The computations appear less

sensitive to the change in angle, returning fluctuation levels similar to those of the vertical case. The extended $k-\varepsilon$ model, with additional $\overline{\theta^2}$ and ε_θ transport equations, not shown here, returns higher fluctuation levels at both angles.

For the 5° cavity, Figure 12 shows comparisons between predicted $k-\varepsilon$ and LES profiles of the wall-parallel velocity and the mean temperature along the cold side. The temperature variation is well reproduced by all models. The $k-\varepsilon$ wall-parallel velocity variations are also close to those of the LES study, with the AWF version leading to closer agreement. Corresponding turbulent kinetic energy comparisons, Figure 13, present a different picture. The LES predictions suggest that along the cold wall there are high turbulence levels over the middle of the cavity with practically laminar flow near the end walls. This trend is returned by the computations, but the k levels are underestimated. The SWF results in the poorest agreement with the LES mean velocity variation. Finally local Nu comparisons along the hot wall of the 5° cavity, Figure 14, show practically no difference between any of the $k-\varepsilon$ predictions and the LES data. They all show high Nu levels near the bottom end wall, where the re-circulating motion, Figure 6, transports the cold fluid, and a gradual reduction toward the top end as the fluid transported upwards heats up. The close agreement with LES suggests that because turbulence levels are low, due to stable stratification, they have only a minor effect on the flow and thermal development at this Rayleigh number.

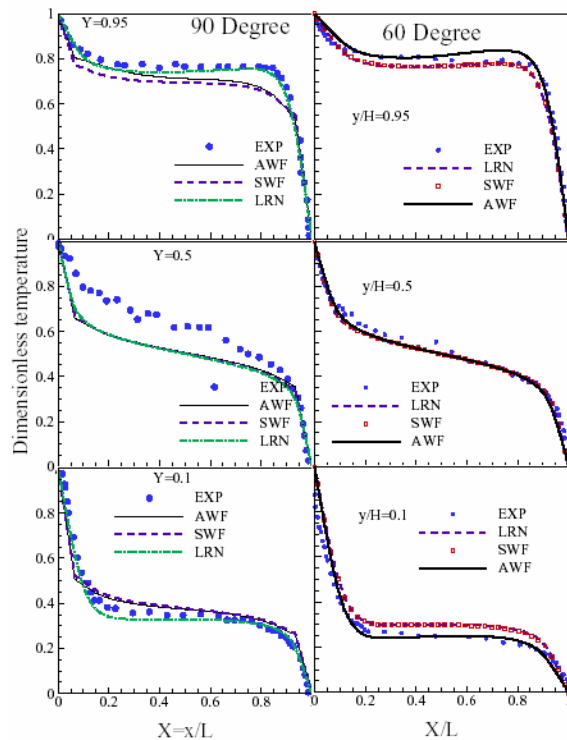


Figure 7. Mean temperature comparisons for 90° and 60° tall cavities. $Ra=0.8 \times 10^6$.

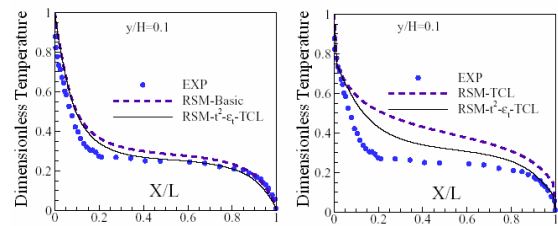


Figure 8. Mean temperature comparisons, using second-moment closures, for the 60° tall cavity. $Ra=0.8 \times 10^6$.

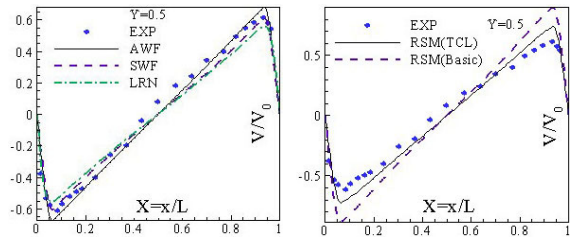


Figure 9. Vertical velocity variation along the mid-horizontal line. Tall 90° cavity, $Ra = 0.86 \times 10^6$.

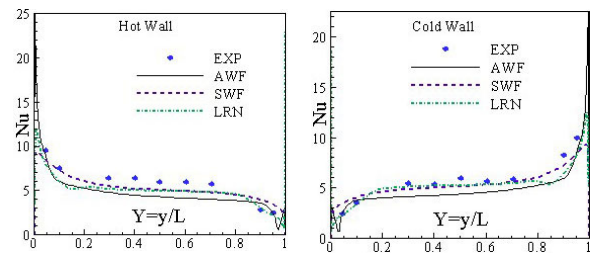


Figure 10. Local Nusselt number variation over the cold and hot walls of the vertical tall cavity. $Ra = 0.86 \times 10^6$.

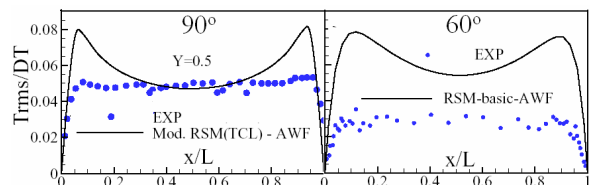


Figure 11. Temperature variance profiles across the cavity at mid-height $Y=0.5$. $Ra = 0.86 \times 10^6$.

CONCLUDING REMARKS

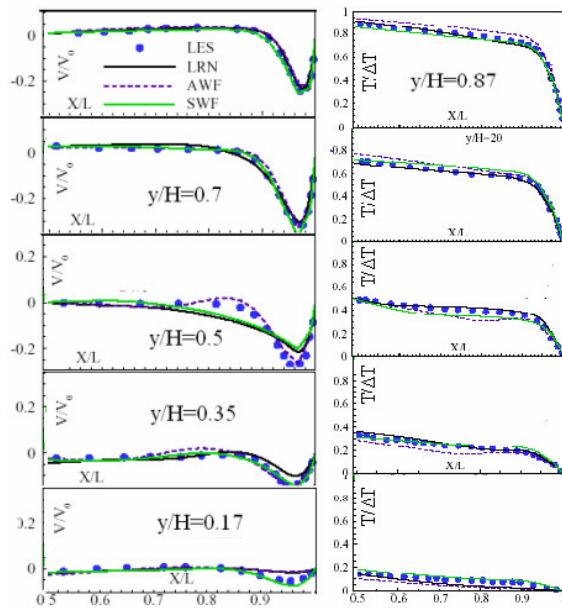
From the comparison of the predictions for the four buoyant flow test cases, it can be concluded that the introduction of the more elaborate analytical wall function (AWF) generally improves the flow and thermal predictions. It thus provides a cost-effective strategy for the near wall modelling of buoyant turbulent flows. Indeed, for the first test case, where the flow is only turbulent within the boundary layer regions, the AWF approach has been shown to be superior to the more expensive low-Re model, which returns completely laminar flow.

The AWF strategy has been combined with more refined models for the Reynolds stresses, such as the two-component-limit (TCL) second-moment closure and also more sophisticated models for the turbulent heat fluxes, such as the algebraic model of Hanjalic et al (1996) based

on additional transport equations for $\overline{\theta^2}$ and ε_θ . This has been shown to further improve the Nusselt number predictions, especially over the horizontal walls of the cavities, and to lead to more reliable predictions of the dynamic and thermal turbulent fields.

For tall differentially heated cavities with either vertical heated walls or inclined at moderate angles to the vertical, the $k-\varepsilon$ model predictions are in close agreement with measurements of the mean velocity, temperature and local Nusselt number. The RSM models display some deficiencies, with the Basic version over-estimating velocity peaks at mid-height and the TCL over-estimating the turbulent mixing near the end walls. The RSM predictions of temperature variance are superior to those of the $k-\varepsilon$, but are still not sensitive to the effect of angle of inclination.

Flow in the 5° inclined cavity is strongly affected by stable stratification. The AWF version of the $k-\varepsilon$ successfully reproduces the LES mean flow and temperature fields, but under-estimates the LES k levels. All models reproduce the LES local Nu variation, which suggests that the low levels of turbulence present have only a minor effect on wall heat transfer.



a) Wall-parallel mean velocity b) Mean temperature
 Figure 12. Mean flow and thermal comparisons along the cold wall of the 5° inclined cavity. $Ra=0.8 \times 10^6$.

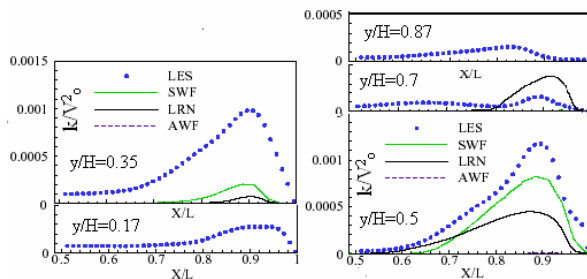


Figure 13. Comparisons of turbulent kinetic energy along the cold wall of the 5° inclined cavity. $Ra=0.8 \times 10^6$.

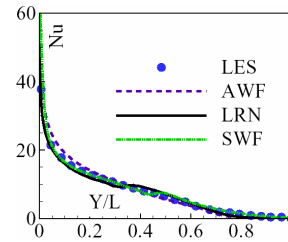


Figure 14. Comparisons of local Nusselt number along the hot wall of the 5° inclined cavity. $Ra=0.8 \times 10^6$.

REFERENCES

Addad Y., Mahmoodilari, M., Laurence, D., (2008), LES and RANS computations of natural convection in a nearly horizontal shallow cavity, Proc. CHT-08, Marakesh.,
 Ampofo, F., Karayiannis, T.G., (2003), Experimental benchmark data for turbulent natural convection in an air filled square cavity, *Int. J. Heat & Mass Transfer*, Vol. 46, pp. 3551–3572.
 Betts, P.L., Bokhari, I.H., (2000), Experiments on turbulent natural convection in an enclosed tall cavity, *Int. J. Heat Fluid Flow*, Vol. 21, pp. 675-683.
 Craft, T.J., Gerasimov, A.V., Iacovides, H., Launder, B.E., (2002), Progress in the generalization of wall-function treatments, *Int. J. Heat Fluid Flow*, Vol. 23, pp. 148-160.
 Craft, T.J., Gerasimov, A.V., Iacovides, H., Kidger, J.W., Launder, B.E., (2004), The negatively buoyant turbulent wall jet: performance of alternative options in RANS Modelling, *Int. J. Heat Fluid Flow*, Vol. 25, pp. 809-823.
 Craft, T.J., Launder, B.E., (2001), Applications of TCL modelling strategy in engineering and environmental flows, Proc. of the 2nd Int. Symp. on Advances in Computational Heat Transfer, Queensland, Australia.
 Dafa'Alla, A.A., Betts, P.L., (1996), Experimental study of turbulent natural convection in a tall cavity, *Experimental Heat Transfer*, Vol. 9, pp. 165-194.
 Dol, H.S., Hanjalic, K., Kenjeres, S., (1997), A comparative assessment of the second-moment differential and algebraic models in turbulent natural convection, *Int. J. Heat Fluid Flow*, Vol. 18, pp. 4-14.
 Esteifi, K., (2009), Personal communication.
 Gibson, M.M., Launder, B.E., (1978), Ground effects on pressure fluctuations in the atmospheric boundary layer, *J. Fluid Mech.*, Vol. 86, pp. 491–511.
 Hanjalic, K., (1994), Achievements and limitations in modelling the computation of buoyant turbulent flows and heat transfer, 10th Int. Heat Transfer Conference.
 Hanjalic, K., Kenjeres, S., Durst, F., (1996), Natural convection in partitioned two-dimensional enclosures at higher Rayleigh numbers, *Int. J. Heat Mass Transfer*, Vol. 30, pp. 1407-1427.
 Ince, N.Z., Launder, B.E., (1989), On the computation of buoyancy-driven turbulent flows in rectangular enclosures, *Int. J. Heat Fluid Flow*, Vol. 10, pp. 110-117.
 Kenjeres, S., Hanjalic, K., (1999), Transient analysis of Rayleigh-Benard convection with a RANS, model, *Int. J. Heat Fluid Flow*, Vol. 20, pp. 329-340.
 Launder, B.E., Sharma, B.I., (1974), Application of the energy-dissipation model of turbulence to the calculation of flow near a spinning disc, *Lett. in Heat Mass Transfer*, Vol. 1, pp. 131-138.